

Mathematical Modeling of the Synergetic Effect between Radiotherapy and Immunotherapy

^{1,2*}Yixun Xing, ^{3*}Casey Moore, ³Debabrata Saha, ^{1,3}Dan Nguyen, ^{1,4}MaryLena Bleile, ^{1,3}Xun Jia, ³Robert Timmerman, ^{1,3,#}Hao Peng, ^{1,3,#}Steve Jiang

¹Medical Artificial Intelligence and Automation Laboratory, University of Texas Southwestern Medical Center, Dallas, TX, 75390, USA

²University of North Texas, Denton, TX, 76205, USA

³Department of Radiation Oncology, University of Texas Southwestern Medical Center, Dallas, TX, 75390, USA

⁴Department of Statistical Science, Southern Methodist University, Dallas, TX, 75275, USA

* These authors contributed equally to this work.

To whom correspondence should be addressed.

E-mail: hao.peng@utsouthwestern.edu, steve.jiang@utsouthwestern.edu

Abstract

Achieving effective synergy between radiotherapy and immunotherapy is critical for optimizing tumor control and treatment outcomes. To explore the underlying mechanisms of this synergy, we have investigated a novel treatment approach known as personalized ultra-fractionated stereotactic adaptive radiation therapy (PULSAR), which emphasizes the impact of radiation timing on treatment efficacy. However, the precise mechanism remains unclear. Building on insights from small animal PULSAR studies, we developed a mathematical framework consisting of multiple ordinary differential equations to elucidate the temporal dynamics of tumor control resulting from radiation and the adaptive immune response. The model accounts for the migration and infiltration of T-cells within the tumor microenvironment. This proposed model establishes a causal and quantitative link between radiation therapy and immunotherapy, providing a valuable in-silico analysis tool for designing future PULSAR trials.

Keywords: Immunotherapy; Personalized ultra-fractionated stereotactic adaptive radiation therapy (PULSAR); T-cell migration; T-cell infiltration; Mathematical modeling.

1. Introduction

The integration of radiation therapy and immunotherapy has emerged as a pivotal approach in the realm of tumor management, leading to improved patient outcomes and enhanced quality of life. This convergence of advances in both physics and biology has given rise to the burgeoning field of radio-immunotherapy, with numerous ongoing trials [1]–[3]. However, these scientific strides have also ushered in a host of new and significant questions. These include inquiries about the optimal radiation dosing scheme for stimulating an immune response, the timing of immunotherapy administration in relation to radiation, and the integration of radiation therapy into the era of personalized precision medicine.

A novel paradigm known as personalized ultra-fractionated stereotactic adaptive radiation therapy (PULSAR), involves the delivery of radiation in ablative doses, with intervals spanning weeks or months, in contrast to the daily fractions commonly employed in clinical practice. This extended time between radiation doses enables adaptation to changes within the tumor, allowing for potential synergetic interaction with immunotherapies. Preliminary preclinical investigations into PULSAR in tandem with immunotherapy have already underscored the impact of radiation scheduling on therapeutic efficacy. Notably, these studies revealed significant benefits when radiation was administered either as a single fraction or separated by ten days, whereas no similar benefit was observed for radiation pulses separated by just one day [4].

Although numerous prior studies have delved into the potential impact of radiation timing in standalone radiotherapy such as stereotactic ablative radiotherapy (SABR), similar research in the realm of radioimmunotherapy remains relatively scarce. It is indeed a challenging task that involves many complex biological processes. To name a few, irradiated T-cells assume a critical role in controlling tumor growth post-radiation therapy. The tumor microenvironment may offer protection to irradiated T-cells, which would otherwise undergo rapid demise elsewhere in the body [5]. Moreover, radiation may also exert immune-inhibitory effects, a factor that must be carefully considered when pairing it with immunotherapy.

Our primary focus is to develop a mathematical model that can model the observed PULSAR effect in the experimental outcomes. The PULSAR effect encompasses not only improved tumor control with radiation pulses separated by one day, compared to a ten-day interval, in the absence of immunotherapy but also a reversed outcome in the presence of immunotherapy. Several representative studies on modeling tumor growth and control are briefly presented below. A top-down model was constructed to depict tumor growth while synchronizing radiotherapy and inhibitors of the PD1-PDL1 axis and the CTLA4 pathway [6]. This model was later simplified and adapted to explore the effects of single- and multiple-fraction schemes with 1-methyl tryptophan [7]. In another study, immune response during and after radiotherapy was modeled to analyze the growth of tumors in immune limited and immune escape modes [8]. Another mathematical model was built to simulate and predict the response of non-small cell lung cancer patients

to combined chemo- and radiotherapy using overall survival data from clinical trials [9]. Kosinsky et al. [10] developed a quantitative pharmacologic model that illustrates the cancer immunity cycle, incorporating radiation treatment and therapeutic blockade of PD1 or PDL18. While comprehensive, this model requires a large number of parameters, potentially leading to overfitting issues. Such an approach was also applied to capture tumor dynamics and predict median clinical responses to monotherapy, combination, and sequential therapy involving the blockade of inhibitory effects by CTLA4, PD1, and PDL1 [11]. Another bottom-up computational model was used to investigate tumor response solely to anti-PD1 antibodies, employing a minimal number of four parameters [12]. Additionally, Sung et al. published a quantitative model outlining the immunosuppressive and immune-stimulating effects induced by radiation therapy [13]. However, this model focused on simulating fractionation strategies without considering any specific immunotherapy modalities.

Despite these promising results, the optimal scheduling of fractionation in the presence of immunotherapy remains a relatively unexplored territory, particularly in the context of PULSAR. It is thus imperative to unravel the intricate processes underlying PULSAR and optimize its synergy with immunotherapy accordingly. In this study, we developed a discrete-time mathematical framework and validated its performances based on the experimental results of mouse studies, taking into account the migration and infiltration of T cells as a function of both dose and time.

2. Methods

2.1 Small animal experiments

All animal procedures were performed following the animal experimental guidelines set by the Institutional Animal Care and Use Committee of the University of Texas Southwestern Medical Center. Female C57BL/6J mice were purchased from Charles River or Jackson Laboratories at six to eight weeks old. Lewis lung carcinoma (LLC) was derived from lung cancer of the C57BL/6 line. Tumor cells were injected subcutaneously on the right leg of mice. Mice were administered (i.p) α -PD-L1 (200 ug) or anti-CD8 agent (200 ug) with different schedules for each group (see Figure A1). Tumor-bearing mice were anesthetized using isoflurane and irradiated with 10 to 40 Gy according to different schedules. Local irradiations were conducted on a dedicated x-ray irradiator (X-RAD 32, Precision X-ray, Inc.). Various collimator sizes were developed to form the field of view, depending on tumor size. The mouse was positioned such that the source-to-tumor surface distance was 20 cm and the tumor was in the center of the x-ray beam. The energy of the x-ray was set to 250 kVp and the current was set to 15 mA for irradiation. The dose rate under this condition was 19.468 Gy/min, which was calibrated using a PTW 31010 ionization chamber and a PTW UnidosEelectrometer (PTW North America Corporation, New York, NY) following the AAPM TG-61 protocol.

The mice were randomized to treatment groups when tumors reached 150 to 200 mm³. Generally, the initial dose of α -PD-L1 or isotype control was applied two or three days before the first radiation, on the day of the initial radiation, and then subsequently every other day for a period. The tumor volumes were measured by length (x), width (y), and height (z) and calculated as tumor volume = xyz/2. When the tumor volume was over 1500 mm³, or the mouse had significant ulceration in the tumor, the mouse reached the survival endpoint and was euthanized. The censored data were then treated with an imputation method [14], [15], followed by the computation of the mean of each treatment group. The data were then partitioned into training and testing datasets, each containing twelve distinct treatment groups. The training data were used to estimate the model parameters while the testing data were held aside for model validation.

2.2 Model overview

Our framework includes the dynamics of three populations, including two types of T-cells and tumor cells as exemplified in **Figure 1**. First, through a chain reaction of other biological pathways such as STING, radiation therapy (RT) recruits new T-cells to the tumor site and stimulates their filtration, in addition to killing T cells along with tumor cells. Second, tumor growth is regulated by the immune response orchestrated by effector T cells, which can be either enhanced by the checkpoint inhibitor antibody (anti-PD-L1) or suppressed by a monoclonal antibody (anti-CD8). More details are described in Equations (1)-(6).

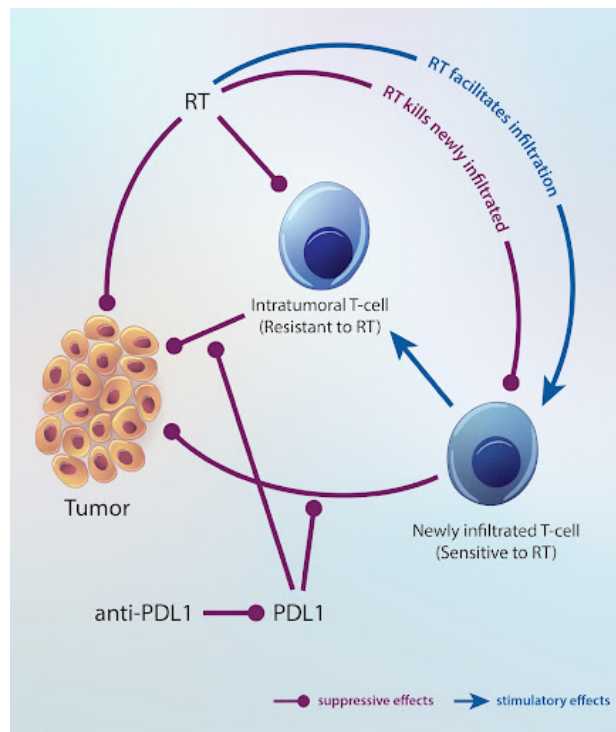


Figure 1. The interactions between the populations with immunosuppressive (red dot-headed lines) and stimulatory (blue arrows) effects.

- The tumor growth dynamics follow Equation (1), where T_n is the tumor volume on day n and grows exponentially to T_{n+1} at a rate μ when no other interference is present. S_n is the survival probability of the tumor upon radiation on day n . Z_n denotes the anti-tumor effect associated with T cells.

$$T_{n+1} = S_n T_n e^{\mu - Z_n} \quad (1)$$

$$S_n = e^{-(\alpha d_n + \beta d_n^2)} e^{-\gamma R_n (\alpha d_n + \beta d_n^2)} \quad (2)$$

$$R_{n+1} = \min(\tau R_n + (1 - S_n), 1) \quad (3)$$

- Equation (2) stems from the standard linear-quadratic model with modifications to incorporate the cumulative effects tied to previous fractions. In other words, the elapsed time matters and a “memorizing” mechanism occurs. The original linear-quadratic term is multiplied by an additional factor due to increased radio-sensitivity post-irradiation. R_n in Equation (3), with an initial value of 0 i.e., $R_0 = 0$ on day 0, along with a coefficient γ indicates the accumulated effect due to a fraction administered on day n , which decays daily by a factor of τ . Accordingly, the subsequent effect, R_{n+1} , is determined jointly by two elements. One is proportional to the strength of the prior radiation $(1 - S_n)$, and the other is the value of formerly accrued effect τR_n . A prior pulse (or fraction) administered in either a higher dosage or a shorter duration would yield greater influence on the survival probability of the next fraction. The term $S_n = e^{-(\alpha d_n + \beta d_n^2)}$ neglects any effect from prior fractions, and only depends on instantaneous dose. After introducing the correction term $e^{-\gamma R_n (\alpha d_n + \beta d_n^2)}$, the survival probability incorporates the impact of previous pulse/fraction, as a form of “increased radio-sensitivity” (see more explanation in the Discussion section).

- Equation (4) models the dynamics of two components, the existing intratumoral T cells (W_{tum}) and newly infiltrated group (W_{new}), which have their own contribution in enhancing the immune response and tumor control (ω_1 and ω_2). The effect of these two components was active only after the administration of anti-PD-L1 and lasted for seven days (e.g., the piecewise nature).

$$Z_n = \begin{cases} \omega_1 W_{tum,n} + \omega_2 W_{new,n} & \text{if anti-PD-L1 is present} \\ 0 & \text{otherwise} \end{cases} \quad (4)$$

- To reflect different responses to radiation between the newly infiltrating immune effector cells W_{new} and more RT-resistant intratumoral tumor T-cells W_{tum} [5], different rates (ϕ_1, ϕ_2) were expected in Equations (5) and (6). In addition, the conversion between W_{new} and W_{tum} happened at an intrinsic rate λ ,

and at the same time the W_{new} subpopulation increased by an amount of ρ due to post-radiation recruitment. The reason why chose an instantaneous is that we consider only immediate effects that begin rapidly after radiation therapy (e.g., within hours rather than days). The generation of T cells as a result of radiation therapy is a complex process that can vary widely depending on several factors. Some tumors may be more immunogenic, leading to a stronger T cell response after radiation. Alternatively, a higher dose may stimulate the release of more tumor-associated antigens and lead to the recruitment of more T cell response. For simplicity, ρ is assumed to be constant in our current study.

$$W_{tum,n+1} = \lambda W_{new,n} + W_{tum,n} e^{-\phi_1 d_n} \quad (5)$$

$$W_{new,n+1} = \begin{cases} (1 - \lambda)W_{new,n} e^{-\phi_2 d_n} + \rho & \text{if radiation is applied} \\ (1 - \lambda)W_{new,n} e^{-\phi_2 d_n} & \text{otherwise} \end{cases} \quad (6)$$

2.3 Model fitting and validation

The model fitting procedure and simulations were implemented in R. Simulated annealing [16] was applied to optimize parameters using the group means of the training data and mean square error (MSE) as a loss function. In each iteration of the optimization procedure, Equations (1)-(6) were computed sequentially to generate the daily tumor volume. The free parameters, along with the initial tumor size T_0 , were initialized as summarized in Table 1 **Error! Reference source not found.** For all groups, the initial estimate of tumor volume was set to one, $T_0 = 1 \text{ mm}^3$. T_0 of each group was adjusted individually to factor in both inter-group and inter-animal variations in the experiment.

Table 1 Parameter space and initial values

Parameter	Lower	Upper	Initial Value for Optimization
α	0	1	0.01
β	0	1	0.0046
ω_1	0	1	0.0005
ω_2	0	1	0.0072
ϕ_2	0	1	0.946
λ	0	1	0.205
ρ	0	100	4.3
$W_{new,0}$	0	100	1
ϕ_1	0	1	0.349

$W_{tum,0}$	0	100	2
μ	0	1	0.1813
γ	0	10	0.15
τ	0	0.9	0.9
T_0	1	10	1

On days when volume measurements were conducted, we collected experimental data and compared the observed tumor size between measurements with simulation results to calculate the Mean Squared Error (MSE) for the training data. The fitting process continued until convergence was achieved. Three fitting procedures were tested as described below:

- 1) Modeling with predetermined and fixed values of α and β at 0.23595 and 0.036284, respectively. This was followed by estimating all other parameters.
- 2) Estimating all parameters by fitting groups sequentially in three stages. First, we fitted the tumor growth rate μ within the 0Gy group without anti-PD-L1 and T_0 . Second, with μ fixed from the previous stage, α , β , τ , and γ , along with group-wise T_0 , were calculated from regimens involving only RTs, such as the groups 10Gyd0d1, 10Gyd0d10, 10Gyd0d1d10d11, 10Gyd0d20, and 10Gyd0d1d20d21. In the final optimization step, we used the above estimates of α , β , τ , and γ as initial values. In this step, group-wise T_0 and all parameters, except the fixed μ , were assessed using all available data except for the 0Gy group.
- 3) Simultaneously estimating all parameters by fitting all treatment groups.

It is important to highlight that we discovered that the simultaneous estimation of all parameters using the complete dataset yielded superior results when compared to two alternative methods. Therefore, only the results of the simultaneous estimation are presented in this manuscript.

3. Results

3.1 Experimental results and PULSAR effect

To demonstrate the PULSAR effect, we will summarize key findings from the animal studies. In this context, we will emphasize the prominent trend in Figures 2 and 3, while presenting specific quantitative results alongside the simulation outcomes in section 3.2.

(20Gyd0, 10Gyd0d1, 10Gyd0d10, and 10Gyd0d4): All these treatment regimens received an identical radiation dose. Those administered with radiation at closer time intervals had slightly different responses to anti-PD-L1. An intriguing observation is the divergence between the solid and dashed blue lines in

20Gyd0 (receiving the lowest anti-PD-L1), 10Gyd0d10, but not in the case of 10Gyd0d4 or 10Gyd0d1. This suggests the presence of immunologically significant processes occurring between days 1 and 10, which can be disrupted by a 10Gy dose and subsequently diminish the cumulative effectiveness of anti-PD-L1.

(20Gyd0d10, 15Gyd0d10): An additional advantage of immunotherapy is apparent when a higher radiotherapy dose is administered at a 10-day interval. The two curves exhibit a striking similarity, while the 15Gyd0d10 group shows relatively inferior tumor control. This extended timeframe allows for enhanced immune cascades and the arrival of different types of cells to signal and bolster the overall anti-tumor immune response.

(10Gyd0d10 and 10Gyd0d1d10d11): The increased radiotherapy dose should typically result in better tumor control. In the 10Gyd0d1d10d11 group, the tumor still has a 10-day interval between radiation treatments but receives a higher cumulative radiation dose, always followed by a second dose the day after the first. However, the difference between the solid blue and dashed blue line is less in the 10Gyd0d1d10d1 group, relative to the 10Gyd0d10 group. In our view, this is likely due to the fact that some immune cells were infiltrating the tumor in the first 24 hours after radiation and may be killed by the second dose when given on d1.

(10Gyd0d10 and 10Gyd0d20): The PULSAR effect is evident in the former scenario but not in the latter. In the 10Gyd0d20 group, there is a less pronounced benefit from additional PD-L1 when the administration is delayed for 20 days. This is likely because the tumors are growing rapidly and require an additional radiation dose primarily to control tumor growth. A single 10Gy dose, in combination with immunotherapy alone, may not suffice. It seems there's a fine balance between achieving a state of equilibrium that allows synergy to manifest and enabling radiotherapy to take a more proactive role in controlling tumor growth.

(10Gyd0d1d10d11, 10Gyd0d1d20d21, 40Gyd0): All three regimens deliver the same cumulative radiation dose. The most effective tumor control is observed in the 40Gyd0 group, where radiotherapy is administered all at once. Setting aside toxicity and side effects, the PULSAR effect is observed except in the 10Gyd0d1d20d21 group. This implies either that the immune response to a single higher dose is superior to lower doses or that the subsequent 3x10Gy treatments worsen the outcome.

Below are two additional observations to note. First, in all the figures, the clear separation between the solid blue and dashed blue lines doesn't occur until around day 10, which coincides with the delivery of the second radiotherapy dose. This delay in response is expected in LLC, a tumor that is inherently resistant to immunotherapy. This highlights the role of radiotherapy in altering the tumor immune microenvironment and triggering cascades of immune responses. The 10-day lag suggests the involvement of lymph nodes, as the priming of a new immune response through a lymph node typically takes around 7-10 days. Furthermore, the difference between 15Gyd0d10 and 15Gyd0d10-CD8 serves as confirmation of the

participation of CD8+ T cells in the anti-tumor immune response, thereby validating the utility of our model based on T cell dynamics.

3.2 Modeling results

The procedure of simultaneously estimating all parameters using the entire dataset produces the best performance, achieving a root mean squared error (RMSE) of 320 mm³ in the training data. Overall, a good alignment of fitted results to experiment data is observed. It is important to note that, in the current phase, our primary focus is on replicating the observed PULSAR effect in the experimental data rather than placing a strong emphasis on quantitative aspects.

(10Gyd0d1, 10Gyd0d10, 10Gyd0d20): When comparing the solid blue and red lines, there is a consistency between experimental and model-based tumor growth. The measured tumor volumes on day 15 are 497 mm³ (the 10Gyd0d1 group), 1100 mm³ (the 10Gyd0d10 group), and 1514 mm³ (the 10Gyd0d20 group), while their respective simulated counterparts are 276 mm³, 728 mm³, and 1615 mm³. More importantly, the modeling results underscore the most prominent efficacy of anti-PD-L1 when there's a ten-day gap between the two radiation fractions. In cases where the fraction interval of the split course is either just one day or as long as 20 days, the benefit from anti-PD-L1 is minimal. For the 10Gyd0d10 with anti-PD-L1 group, the simulated tumor volume on day 18 is 257 mm³, significantly lower than the 1392 mm³ without anti-PD-L1. Conversely, the modeling outcomes 280 mm³ (the 10Gyd0d1 with anti-PD-L1 group) and 1023 mm³ (the 10Gyd0d20 with anti-PD-L1 group) on day 15 are quite similar to those without anti-PD-L1, 276 mm³ (the 10Gyd0d1 group) and 1615 mm³ (the 10Gyd0d20 group).

(10Gyd0d1d10d11, 10Gyd0d1d20d21): The estimated tumor volumes generally align with the actual ones. On day 23, the observed and estimated tumor volumes are 703 mm³ and 718 mm³ for the 0Gyd0d1d10d11 group and 1506 mm³ and 1508 mm³ for the 0Gyd0d1d20d21 group. Furthermore, the model predicts a tumor volume of 460 mm³ in the 10Gyd0d1d10d11 with anti-PD-L1 group, showcasing the PULSAR effect.

The model also demonstrates strong accuracy in the testing groups, with an RMSE of 287 mm³. The same patterns as described earlier are observed in groups with varying time intervals.

(10Gyd0d4, 15Gyd0d10, 15Gyd0d10-CD8, 20Gyd0): The modeling curves approximate the measurement curves well in these groups. The tumor volumes are 1011 mm³ (the 10Gyd0d4 group), 1294 mm³ (the 15Gyd0d10 group), 969 mm³ (the 15Gyd0d10-CD8 group), and 1009 mm³ (the 20Gyd0 group) on day 22. The corresponding modeling results are 1015 mm³, 1104 mm³, 930 mm³, and 1057 mm³. Due to the short interval of four days in the 10Gyd0d4 group, the impact of anti-PD-L1 on inhibiting tumor growth is exceedingly modest, as evidenced by both a measurement of 1125 mm³ and a simulated volume of 1109 mm³ on day 22. In the case of the 15Gyd0d10 group, the simulation reveals a noteworthy contrast

in tumor volumes with anti-PD-L1 (210 mm³) and without anti-PD-L1 (1104 mm³) on day 22, with a difference of 894 mm³. A comparable disparity of 599 mm³ is indeed observed in the experimental data. In the experiment data, the 15Gyd0d10-CD8 group with anti-PD-L1 (1282 mm³) differs from that without anti-PD-L1 (969 mm³) in tumor volume on day 22 by 313 mm³, which is estimated to be a difference of 17 mm³ (913 mm³ versus 930 mm³). The modeling result appears to differ from the actual value in this radiation regime with the presence of anti-PD-L1. This discrepancy arises from the model's challenge in accurately predicting increased tumor volume control penalty when the anti-PD-L1 is present, as compared to when it is not. However, our model showcases that the depletion of T cells, as a result of anti-CD8 administration, also accelerates tumor growth, even when fractions are properly spaced, in the presence of a checkpoint inhibitor.

(20Gyd0d10, 40Gyd0): On day 22, the simulated differences in tumor volume are 134 mm³ (92 mm³ for 20Gyd0d10 with anti-PD-L1 versus 226 mm³ for 20Gyd0d10 without anti-PD-L1) and 113 mm³ (75 mm³ for 40Gyd0 with anti-PD-L1 versus 188 mm³ for 40Gyd0 without anti-PD-L1). This approximation closely mirrors the observed differences of 298 mm³ and 126 mm³ in the experimental data. Nonetheless, we also observe disparities between experimental outcomes and simulation results in these two scenarios. For instance, noticeable differences between the solid blue and red lines are evident between day -2 and 16 for 40Gyd0 and 20Gyd0d10. This issue remains an unanswered question within our current modeling approach. On one hand, this discrepancy might be attributed to the small tumor volume, which is comparatively less accurately represented in our modeling compared to other groups. On the other hand, it's crucial to understand that the PULSAR effect is a relative metric, and the primary concern lies in the ultimate tumor control achieved at the conclusion of the treatment, rather than the fluctuations throughout the treatment duration.

Table 2 presents the summary of fitting parameters based on the training data. Notably, ϕ_1 exhibits a significantly lower value than ϕ_2 , underscoring the differing sensitivities between tumor T-cells and newly infiltrated T-cells in response to radiation. ω_1 and ω_2 represent the respective contributions of these two distinct T-cell subpopulations. The parameter λ indicates the conversion rate of newly infiltrating effector cells into intratumoral ones. The parameter τ , the decaying rate of 0.886, indicates that the accumulated radiation effect resulting from a single pulse diminishes in about 9 to 10 days. More in-depth explanations of these parameter meanings can be found in the Discussion section.

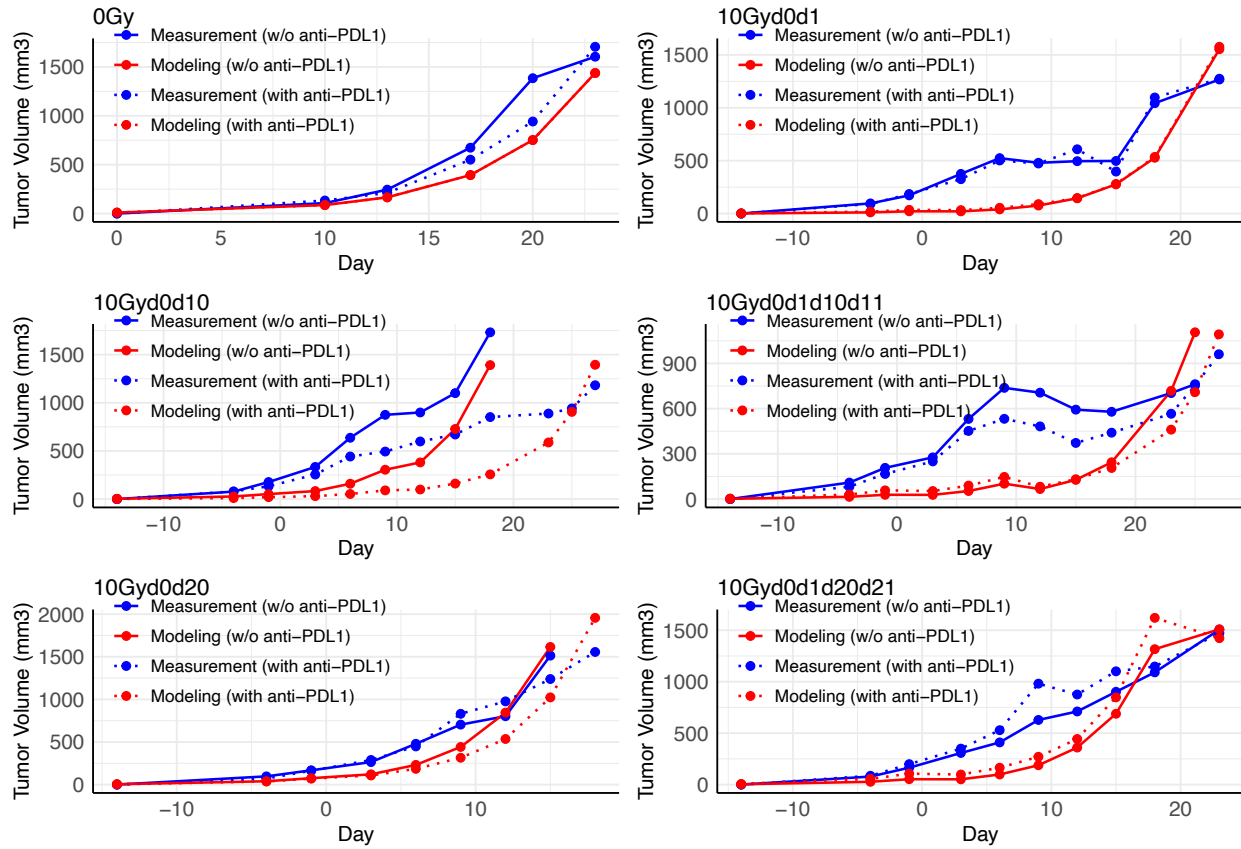


Figure 2. Experimental data (blue) used to estimate the parameters vs simulated tumor growth (red) of groups of different time spacing between the two fractions. In all the above plots, the solid line represents radiotherapy only while the dashed line represents radiotherapy and immunotherapy combined. The 'Day' on x-axis represents the day after the first RT if at least one radiation pulse is administered.

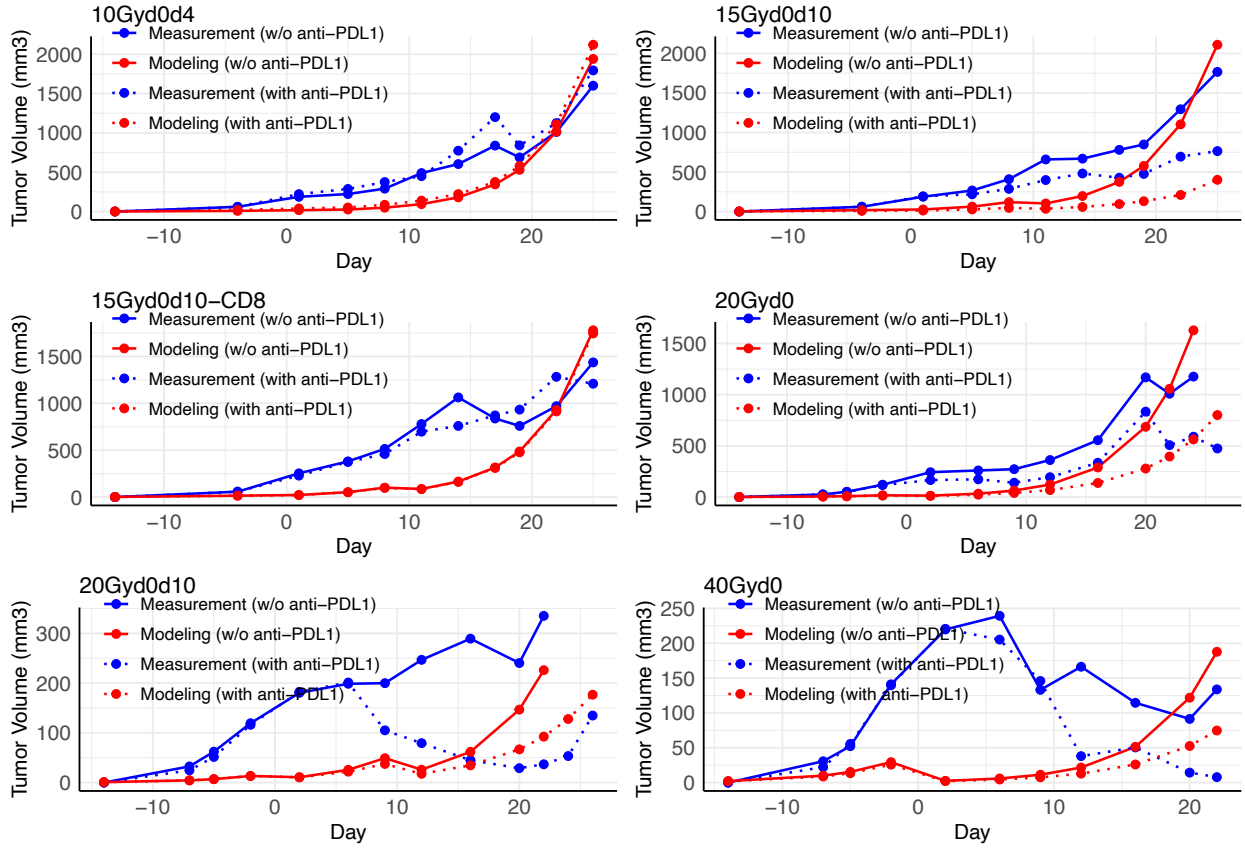


Figure 3. Experimental data (blue) in the testing data set of groups of different time spacing between the two fractions vs simulated tumor growth (red). In all the above plots, the solid line represents radiotherapy only while the dashed line represents radiotherapy and immunotherapy combined. The ‘Day’ on x-axis represents the day after the first RT if at least one radiation pulse is administered.

Table 2. Summary of estimated parameters.

Parameter	Estimate
α	0.0240
β	0.00148
ω_1	0.0235
ω_2	0.0140
ϕ_2	0.964
λ	0.304
ρ	1.707
$W_{new,0}$	0.00001
ϕ_1	0.05205

$W_{tum,0}$	0
μ	0.216
γ	0.883
τ	0.886

3.3 In-silico outcome prediction

Figure 4 shows the simulated tumor growth of six possible treatments including a four-day interval (red), eight-day interval (blue), and twelve-day interval (green) of two radiation pulses, each of 20 Gy (top row) or 30 Gy (bottom row). The initial tumor size is constant for all six groups. For the 20 Gy scenario, the PULSAR effect is most significant when the two pulses are separated by 8 days compared to the counterparts of 4 days and 12 days. For the 30 Gy scenario, the overall tumor volume is much lower due to the high dose. The PULSAR effect is most noticeable when the two pulses are separated by 12 days. Nevertheless, the overall tumor control, in terms of the tumor volume at the endpoint, is found to be the best for 8 days. The results in Figure 4 exemplify the complex relationship between the optimal synergy and dose sequence (or fractionation) of radiotherapy.

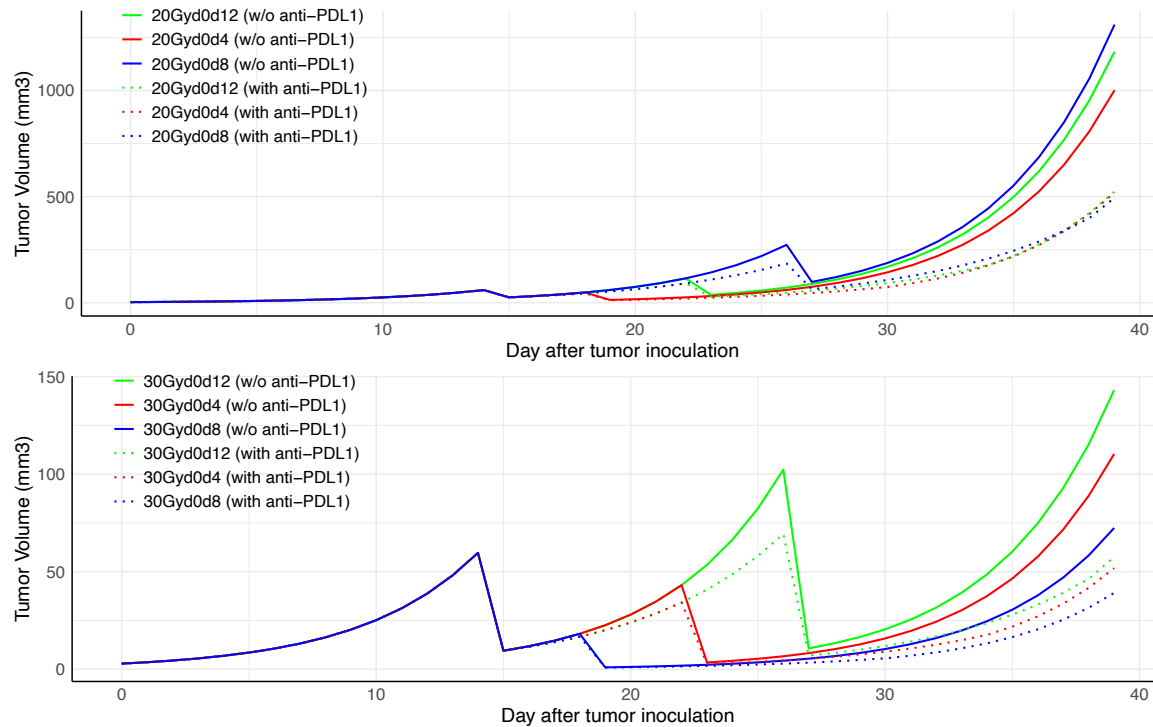


Figure 4. The simulated tumor growth of six possible treatments including a four-day interval (red), eight-day interval (blue), and twelve-day interval (green) of two fractions each of 20 Gy (top) or each of 30 Gy (bottom).

4 Discussion

In this study, we constructed a mathematical framework for modeling the PULSAR effect utilizing a set of ordinary differential equations (ODEs). This framework reveals its potential value for elucidating the temporal dynamics of tumor control, and the impact of both radiation and adaptive immune response, in a qualitative or at most semi-quantitative way. Our framework establishes a causal link between radiation therapy and immunotherapy. The framework can effectively model the tumor progression in the presence of monotherapy or an integrated treatment approach as shown in Figures 2 and 3, for various groups with distinct time intervals of one day, four days, ten days, and twenty days. Additionally, the model can support in-silico studies and generate essential data to address additional research questions related to combined therapy.

The strength of using ODEs for modeling the synergy is demonstrated, with respect to its practical use and generalization capability. The ODEs may appear unsophisticated and overly simplified. However, it is the most basic ODE models that have been most commonly used for practical biological modeling, such as tumor growth models, pharmacodynamics models, and the well-known linear quadratic (LQ) model in radiobiology. Mathematical simplicity is purposely attained with minimal components and parameters. Also, we believe the chosen top-down approach is easier for potential translation into clinical practice. Some parameters, such as τ , ϕ_1 , ϕ_2 , λ , can be validated and fine-tuned through experiments including flow cytometry and molecular imaging technologies. For example, optical imaging tools can be employed to investigate the dynamics of T cells, comprising their migration from lymph nodes to the targeted tumor via the circulatory system and their subsequent infiltration into the tumor.

In our modeling, the “increased radio-sensitivity” is found to be an essential component for the ODEs to achieve high fitting accuracy, through the heuristic terms defined in Eqs. 2 and 3. The original linear-quadratic term is multiplied by the additional terms due to increased radio-sensitivity post-irradiation, depending on two parameters γ and τ in a recursive manner. The cumulative effect of radiation decreases as the time elapses, lasting around ten days corresponding to the decaying coefficient τ . As shown in Figure 3, tumor control is more noticeable in group 10Gyd0d1 without anti-PDL1 (two 10 Gy pulses, day 0 and day 1), compared to group 10Gyd0d10 without anti-PDL1 (two 10 Gy pulses, day 0 and day 10). Nevertheless, two additional questions remain to be answered. First, is there any underlying radiobiological cause possibly linked to the increased radiosensitivity? Second, whether the exponential decay of the cumulative effect of a single pulse linked to cell repair?

Another novel aspect of our study is the integration of T cell dynamics along with pulsed radiation, including the differentiation and conversion of preexisting intratumoral and newly infiltrating T-cells. Multiple investigations have underscored the critical role played by the density and characteristics of tumor-infiltrating T cells in determining the clinical effectiveness of anti-PD-1/PD-L1 therapy. Arina et al. [5] reported that resident T cells present during radiation are more resistant to death and are important for overall tumor control. However, T cells in other compartments of the body are less resistant to radiation. Although the authors did not perform a second dose of radiation 24 hours after the first, we find it an intriguing point for studying the synergy between radiotherapy and immunotherapy. We speculate that newly infiltrated T cells might be more sensitive to the second radiation pulse as they are phenotypically more like the T cells in other areas of the body. This leads to the formulation in Eq. 5. Without taking into account the immunomodulatory effect, the parameter τ results in reduced tumor control for a larger spacing between two pulses (i.e., smaller tumor volume corresponding to 1-day spacing). However, such a pattern is altered after considering the temporal dynamic of T-cells. When the two pulses are spaced ten days apart, the PULSAR effect is observed to be most significant relative to other spacing schemes (1 day, 4 days, 20 days). At the same time, the estimated parameters ϕ_1, ϕ_2, λ support our speculation the T-cell reprogramming is closely tied to the PULSAR effect. Different values of ϕ_1 and ϕ_2 reveal two types of T-cells of different radiosensitivity. A subpopulation of T-cells gradually develops resistance and is converted into intratumoral T-cells, as represented by the parameter λ . Although we do not expect the proposed model to be quantitative, the examination of these parameters increases our confidence in the soundness of the ODE-based modeling approach.

Two plausible biological processes that might explain the maximum PULSAR effect around 10 days are briefly mentioned below. One process is related to Treg. To prevent autoimmune reactions following radiation, Treg cells are recruited to the tumor site and suppress immune response through a number of signaling pathways, such as elevated expression of CTLA4 for suppressing inflammation response of antigen-presenting cells, cytokines IL10 for T helper cells, and TGF- β for cytotoxic T cells. Simultaneously, some Treg cells infiltrate the tumor bed and release type-I interferon gamma, which leads to the upregulation of PD-L1 on the surface of tumor cells. The temporal scale of this last process takes up to several days after radiation. Another process might be related to the homing of T cells. In "hot" tumors, there is a robust immune response characterized by significant immune cell infiltration and activation of immune pathways. Conversely, "cold" tumors such as LLC in our study exhibit limited immune response, with minimal immune cell infiltration and reduced immune activity. In "hot" tumor models, a single radiation dose may be sufficient for maximizing synergy with immunotherapy, as initial priming of the immune response has already occurred due to preexisting tumor immunity. In "cold" tumors, an initial priming dose of radiation is necessary, and thus the PULSAR effect manifests after approximately 10 days.

Our current study presents several limitations which will be addressed in future studies. Firstly, the model development was based on a limited dataset. The small sample size of five to ten subjects in each treatment group indicates a need for recruiting more mice in subsequent studies, to reduce both intra- and inter-group variation. Secondly, in our current study, the definition of synergy relies solely on tumor size, lacking additional information about T cells related to migration and infiltration. A potential remedy involves conducting flow cytometry and optical imaging experiments to better understand the temporal behavior of T cells. Thirdly, our model focuses on the PULSAR effect, not yet taking into account the risk of potential toxicities. As the combined radioimmunotherapy has the potential to result in delayed toxicities, the standard assessment models may not be appropriately suited.

5. Conclusion

The synergistic potential of combining radiotherapy and immunotherapy has a unique role in cancer treatment. In this work, a mathematical model based on multiple ODEs is developed to examine the PULSAR effect, demonstrating good consistency with the experimental findings. One novel aspect is the integration of T cell dynamics along with pulsed radiation, including the differentiation and conversion of preexisting intratumoral and newly infiltrating T-cells. The model lays a good foundation for us to explore the potential therapeutic synergy between radiotherapy and immune checkpoint blockade. To elicit the optimal immune response, our framework will not only help find the optimum dose and fractionation of radiotherapy but also may help optimize the dosing of immune checkpoint inhibitors and the sequence.

Conflict of Interest

The author(s) declare(s) that there is no conflict of interest regarding the publication of this article.

Acknowledgements

This work was supported by National Institutes of Health [grant numbers R01CA237269, R01CA254377, and R01CA258987].

References

- [1] F. Agostoni and F. R. Hirsch, "PACIFIC trial: new perspectives for immunotherapy in lung cancer," *Transl Lung Cancer Res*, vol. 7, no. S1, pp. S19–S24, Feb. 2018, doi: 10.21037/tlcr.2017.12.12.
- [2] A. Bulbul and E. Araujo-Mino, "Reasoning the effect of immunotherapy after chemoradiation in the PACIFIC trial," *Future Oncology*, vol. 15, no. 1, pp. 81–94, Jan. 2019, doi: 10.2217/fon-2018-0464.
- [3] W. G. Breen, K. Leventakos, H. Dong, and K. W. Merrell, "Radiation and immunotherapy: emerging mechanisms of synergy.," *J Thorac Dis*, vol. 12, no. 11, pp. 7011–7023, Nov. 2020, doi: 10.21037/jtd-2019-cptn-07.

- [4] C. Moore *et al.*, “Personalized Ultrafractionated Stereotactic Adaptive Radiotherapy (PULSAR) in Preclinical Models Enhances Single-Agent Immune Checkpoint Blockade,” *International Journal of Radiation Oncology*Biophysics*, vol. 110, no. 5, pp. 1306–1316, Aug. 2021, doi: 10.1016/j.ijrobp.2021.03.047.
- [5] A. Arina *et al.*, “Tumor-reprogrammed resident T cells resist radiation to control tumors,” *Nat Commun*, vol. 10, no. 1, p. 3959, Sep. 2019, doi: 10.1038/s41467-019-11906-2.
- [6] R. Serre *et al.*, “Mathematical Modeling of Cancer Immunotherapy and Its Synergy with Radiotherapy,” *Cancer Res*, vol. 76, no. 17, pp. 4931–4940, Sep. 2016, doi: 10.1158/0008-5472.CAN-15-3567.
- [7] A. Chakwizira, J. Ahlstedt, H. Nittby Redebrandt, and C. Ceberg, “Mathematical modelling of the synergistic combination of radiotherapy and indoleamine-2,3-dioxygenase (IDO) inhibitory immunotherapy against glioblastoma,” *Br J Radiol*, vol. 91, no. 1087, p. 20170857, May 2018, doi: 10.1259/bjr.20170857.
- [8] Y.-B. Cho, N. Yoon, J. H. Suh, and J. G. Scott, “Radio-immune response modelling for spatially fractionated radiotherapy,” *Phys Med Biol*, vol. 68, no. 16, p. 165010, Aug. 2023, doi: 10.1088/1361-6560/ace819.
- [9] C. Geng, H. Paganetti, and C. Grassberger, “Prediction of Treatment Response for Combined Chemo- and Radiation Therapy for Non-Small Cell Lung Cancer Patients Using a Bio-Mathematical Model,” *Sci Rep*, vol. 7, no. 1, p. 13542, Oct. 2017, doi: 10.1038/s41598-017-13646-z.
- [10] Y. Kosinsky *et al.*, “Radiation and PD-(L)1 treatment combinations: immune response and dose optimization via a predictive systems model,” *J Immunother Cancer*, vol. 6, no. 1, p. 17, Dec. 2018, doi: 10.1186/s40425-018-0327-9.
- [11] O. Milberg *et al.*, “A QSP Model for Predicting Clinical Responses to Monotherapy, Combination and Sequential Therapy Following CTLA-4, PD-1, and PD-L1 Checkpoint Blockade,” *Sci Rep*, vol. 9, no. 1, p. 11286, Aug. 2019, doi: 10.1038/s41598-019-47802-4.
- [12] D. Valentinuzzi, U. Simončič, K. Uršič, M. Vrankar, M. Turk, and R. Jeraj, “Predicting tumour response to anti-PD-1 immunotherapy with computational modelling,” *Phys Med Biol*, vol. 64, no. 2, p. 025017, Jan. 2019, doi: 10.1088/1361-6560/aaf96c.
- [13] W. Sung *et al.*, “A tumor-immune interaction model for hepatocellular carcinoma based on measured lymphocyte counts in patients undergoing radiotherapy,” *Radiotherapy and Oncology*, vol. 151, pp. 73–81, Oct. 2020, doi: 10.1016/j.radonc.2020.07.025.
- [14] J. L. Schafer, “Multiple imputation: a primer,” *Stat Methods Med Res*, vol. 8, no. 1, pp. 3–15, Feb. 1999, doi: 10.1177/096228029900800102.
- [15] D. B. Rubin, “The Calculation of Posterior Distributions by Data Augmentation: Comment: A Noniterative Sampling/Importance Resampling Alternative to the Data Augmentation Algorithm for Creating a Few Imputations When Fractions of Missing Information Are Modest: The SIR,” *J Am Stat Assoc*, vol. 82, no. 398, p. 543, Jun. 1987, doi: 10.2307/2289460.
- [16] S. Kirkpatrick, “Optimization by simulated annealing: Quantitative studies,” *J Stat Phys*, vol. 34, no. 5–6, pp. 975–986, Mar. 1984, doi: 10.1007/BF01009452.

Appendix

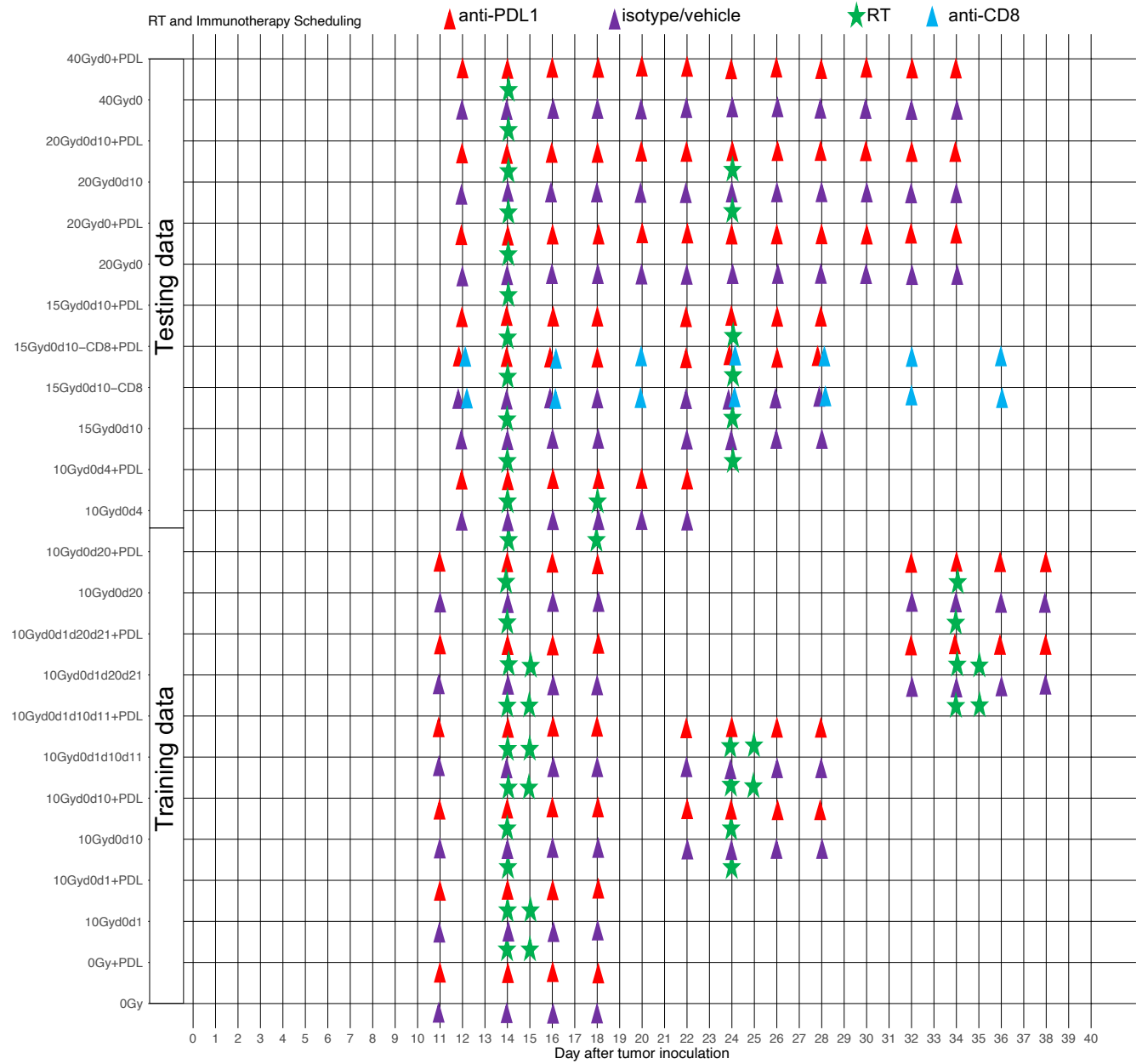


Figure A1. Radiotherapy and immunotherapy scheduling.